Final Report

Millimeter-Wave Holographic Imaging System for Radiating Array Assay and Adjustment

Air Force
Contract Number F49620-97-1-0153
(CU Ref. 01-6884)

L. Wilson Pearson, PI
Department of Electrical and Computer Engineering
Clemson University
Clemson, SC 29634-0915

Februrary 21, 2000

REPORT DOCUMENTATION PAGE

AFRL-SR-BL-TR-00-

0796

1. AGENCY USE ONLY *(Leave blank)*	2. REPORT DATE	3. REPORT TYPE AND DATES COVERED
	February 21, 2000	Final Technical Report 1 Apr 97 to 31 dec 97

4. TITLE AND SUBTITLE
Millimeter-Wave Holographic Imaging System for Radiating Array Assay and Adjustment

5. FUNDING NUMBERS
F49620-97-1-0153

6. AUTHOR(S)
L. Wilson Pearson

7. PERFORMING ORGANIZATION NAME(S) AND ADDRESS(ES)
Department of Electrical & Computer Engineering
Clemson University
Clemson SC 29634-0915

8. PERFORMING ORGANIZATION REPORT NUMBER

9. SPONSORING/MONITORING AGENCY NAME(S) AND ADDRESS(ES)
AFOSR/NM
801 N. Randolph St, Rm 732
Arlington, VA 22203-1977

10. SPONSORING/MONITORING AGENCY REPORT NUMBER
F49620-97-1-0153

11. SUPPLEMENTARY NOTES

12a. DISTRIBUTION AVAILABILITY STATEMENT
Approved for public release; distribution unlimited.

12b. DISTRIBUTION CODE

13. ABSTRACT *(Maximum 200 words)*

This is a final report on equipment purchased under the subject Defense University Research Instrument Program (DUR1P) Grant. The grant involved equipment purchase only, and several items were combined into a single one-of-a-kind system. The following paragraphs provide a summary of the items purchased and a brief description of the custom antenna scanning facility assembled from the specific item of a Cascade Probe Station. Items Purchased: Receiver System; Distributed Downconverter; Synthesizer -20 Gz.1 Opt. H-62; Power Amp (source side)1; mmW. Heads; mmW. Heads; mmW Interface; Sweeper Chassis (for LO source)1 2-20 GHz. Plug-inl Opt. K69; Custom Cascade Probe Station2; Monitor for Control Computer on Cascade System. The First nine items comprise an integrated receiving system. Item 10 is a high precision position controller designed for use in on-wafer testing of integrated circuits. We purchased this system with several items of the test platform deleted and have refitted it as a programmable x-y positioner for high-precision near-field scanning of millimeter wave apertures. Figure 1 shows a picture of this configuration. One can identify a rectangular waveguide oriented vertically. This is the scanning probe. The positioning mechanism of the Cascade Probe Station can be seen below. The antenna under test is positioned above the waveguide and a few wavelengths away, It radiates down toward the waveguide. The system is fully assembled and we have developed software in house to control the system and to perform and scan-plane-to-radiating-aperture field transformations. Operation of the RF systems has been verified in all bands of operation.

14. SUBJECT TERMS	15. NUMBER OF PAGES
	16. PRICE CODE

17. SECURITY CLASSIFICATION OF REPORT	18. SECURITY CLASSIFICATION OF THIS PAGE	19. SECURITY CLASSIFICATION OF ABSTRACT	20. LIMITATION OF ABSTRACT
UNCLASSIFIED	UNCLASSIFIED	UNCLASSIFIED	UL

Introduction

This is a final report on equipment purchased under the subject Defense University Research Instrument Program (DURIP) Grant. The grant involved equipment purchase only, and several items were combined into a single one-of-a-kind system. The following paragraphs provide a summary of the items purchased and a brief description of the custom antenna scanning facility assembled from the specific item of a Cascade Probe Station.

Items Purchased

	Model Number	Item
1.	Hewlett Packard 8530A	Receiver System
2.	Hewlett Packard 85309A	Distributed Downconverter
3.	Hewlett Packard 83620B	Synthesizer -20 Gz.[1] Opt. H-62
4.	Hewlett Packard 8349A	Power Amp (source side)[1]
5.	Hewlett Packard Q85325A	mmW. Heads
6.	Hewlett Packard W85325A	mmW. Heads
7.	Hewlett Packard 85326A	mmW Interface
8.	Hewlett Packard 8350B	Sweeper Chassis (for LO source)[1]
9.	Hewlett Packard 83592B	2-20 GHz. Plug-in[1] Opt. K69
10.	Cascade S12201	Custom Cascade Probe Station[2]
11.	Mag 710	Monitor for Control Computer on Cascade System

Configuration of the System

The First nine items comprise an integrated receiving system. Item 10 is a high precision position controller designed for use in on-wafer testing of integrated circuits. We purchased this system with several items of the test platform deleted and have refitted it as a programmable x-y positioner for high-precision near-field scanning of millimeter wave apertures. Figure 1 shows a picture of this configuration. One can identify a rectangular waveguide oriented vertically. This is the scanning probe. The positioning mechanism of the Cascade Probe Station can be seen below. The antenna under test is positioned above the waveguide and a few wavelengths away. It radiates down toward

the waveguide. The system is fully assembled and we have developed software in house to control the system and to perform the scan-plane-to-radiating-aperture field transformations. Operation of the RF systems has been verified in all bands of operation.

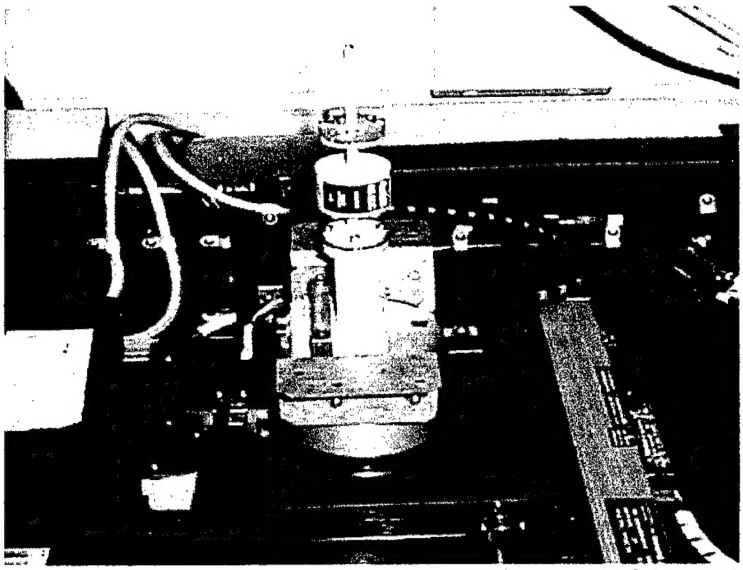

Figure 1. Scanning Probe and x-y positioning mechanism of Near-Field Scanning System. The waveguide probe Operates in R-band (35-50 GHz)

Array Evaluation at Millimeter Wavelengths Employing Planar Near-Field Scanning

J. D. Morsey
Department of Electrical and Computer Engineering
University of Illinois
Urbana, IL 38677

and

L. W. Pearson
Holcombe Department of Electrical and Computer Engineering
Clemson University
Clemson, SC 29634-0915
pearson@ces.clemson.edu

Introduction

The emerging deployment of radiating arrays at millimeter wavelengths introduces new complexity to the task of assaying array performance due to the small size of the array, to the fine tolerances imposed by short wavelength, and the potential inaccesibility of intermediate points in the RF system distributing power through the array. Ransom and Mittra [1] and Lee, *et. al.* [2] have proposed planar near-field scanning as a means of inferring the aperture field across a radiating array by way of standard holographic near-field transformation. Recently, an electro-optic system capable of precise, relatively complete, sampling of near fields has been implemented [3, 4]. The completeness of data in this latter system results from the fact that the sampling is done through the invasion only of a (dielectric) electro-optic probe that is scanned in immediate proximity to the radiating aperture. Proximity to the aperture provides measured fields that include the invisible spectrum of the aperture.

The system that we report here is implemented in the spirit of [1, 2] and provides a scheme that is complementary to the relatively elaborate electro-optical system of [3, 4]. The near-field system is limited, of course, by the fact that invisible spectrum data is lost in a scanning plane that is removed by a few wavelengths from the radiating aperture. On the other hand, as we demonstrate in this presentation, the level of detail retained is adequate to provide assay of amplitude and phase of radiating elements on the order of ten percent in amplitude and fifteen degrees in phase. This level of accuracy can be quite useful in the initial adjustment of a radiating array or in assessing failures.

System Description

Figure 1 shows the test-probe region of the millimeter wave near-field scanning system. The scanning robot is an adapted Summit 12000 probe station. This system provides 1 μm position reproducability, and a scan area of 20.5 by 20.5 cm. The system is implemented with the test aperture directed downward toward the scanning bed of the Summit probe station, and the test probe, and open-ended waveguide, is mounted on the translation head of the probe station. The test mixer is mounted in fixed relationship to

the waveguide probe so that moving cables contain only IF frequencies. This obviates difficulties associated with phase change on flexing cable.

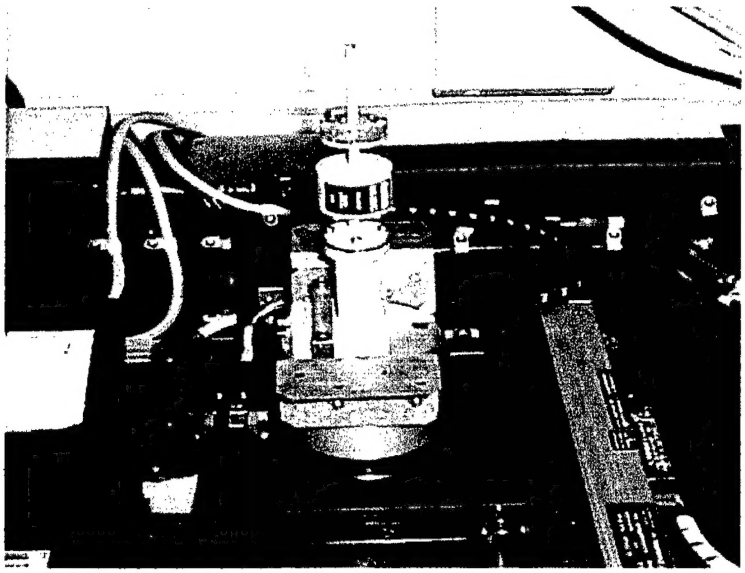

Fig. 1. Translation bed of Summit Probe station with mixer and open-ended waveguide mounted. Absorber used in operation is removed for clarity. The test aperture is mounted overhead above the test probe shown.

The Summit prove station allows vertical (z-axis) adjustment over a 0.55 cm. range. The mounting of the radiating aperture overhead can implemented so as to accommodate additional z-axis adjustment if a particular measurement set suggests it. We typically employ a scanning plan on the order of ten wavelengths from the test aperture. Standard-Fast-Fourier-Transform/back-propagation algorithms are employed to translate data taken in the measurement plane to form an inferred image of the field in the radiating aperture. Of course, if one wishes, far-field patterns can be computed as well.

The angular variation in probe sensitivity must be accounted for in a measurement. Precise calibration through pattern measurement is possible, but we have limited our probe calibration to the analytical calibration of Yaghjian [5].

Information Lost with the Invisible Spectrum

The key limitation of this method is the loss of the invisible spectrum in the field as it propagates over the distance from the radiating aperture to the measuring plane. The invisible spectrum is defined as those constituents of the plane-wave spectrum of the field that exhibit exponential decay in the z direction. Fig. 2 pictures the geometry of a pair of resonant microstrip patches that we employed in a numerical study of the influence of the invisible spectrum. A standard model of the patch as two slot radiators separated by a half wavelength adjusted by fringing correction. For purposes of the computation, the data can be characterized in terms of a single increment parameter, Δ, as shown in the figure.

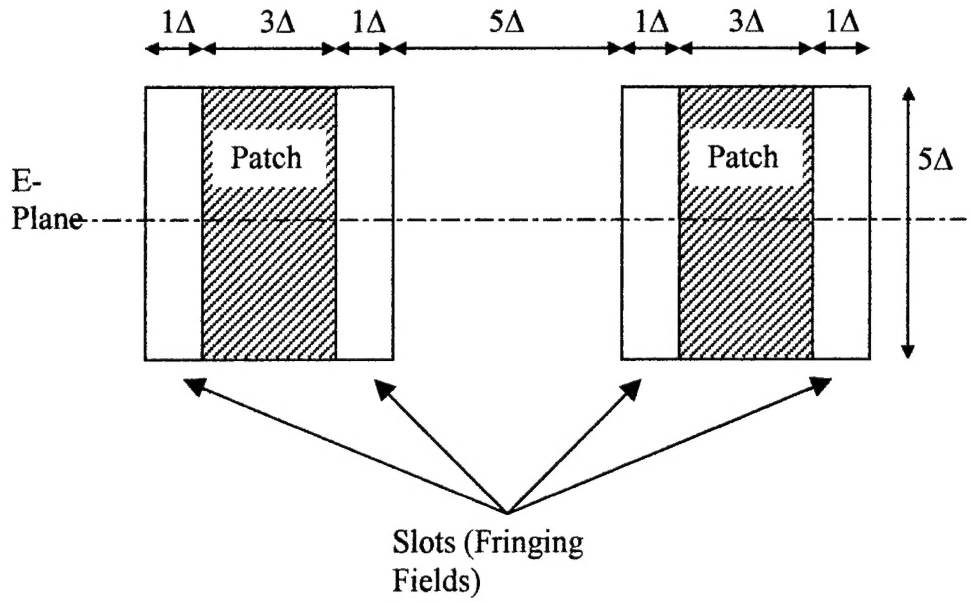

Fig. 2. Geometry of patches employed in computational experiments.

Fig. 3 shows the image of the radiating slots simulated as if the measurement recovered both the visible and the invisible spectrum of the field at the measurement plane.

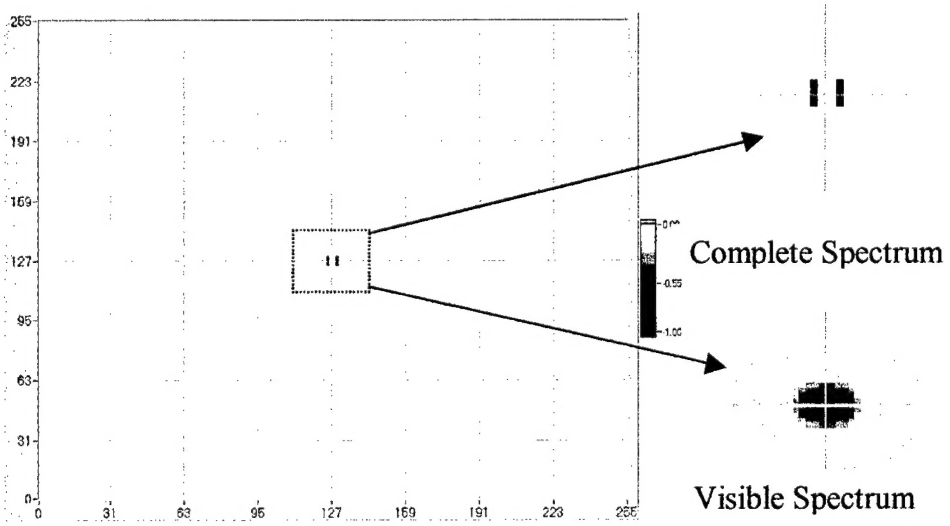

Fig. 3. Simulated reconstructions with complete spectrum and truncation to the visible spectrum alone.

Fig. 4. Shows an image formed from measured data (and hence the visible spectrum only) for a four-element array of patch antennas operating at 34.6 GHz. Fig. 4a. is the radiating plane image formed from near-field data. A 128x128 point scanning plane was measured over a 20.47x20.47cm area (step size of 0.16cm or 0.185λ). The array was separated from the probe by a distance of 7.5cm or 8.65λ. This gave a measured angular spectrum of approximately ±70°. Fig. 4b. shows the image of the same array scanned in the system

of [4]. One sees that the anticipated blurring associated with loss of the invisible spectrum is evident in Fig. 4a. A great deal of detail, including the individual radiating edges and the fields near the microstrip lines in the feed structure is evident in Fig. 4b.

Data presented in the oral presentation indicates that the data associated with Fig. 4a. is adequate to allow one to infer to useful accuracies the amplitude and phase of each operating patch.

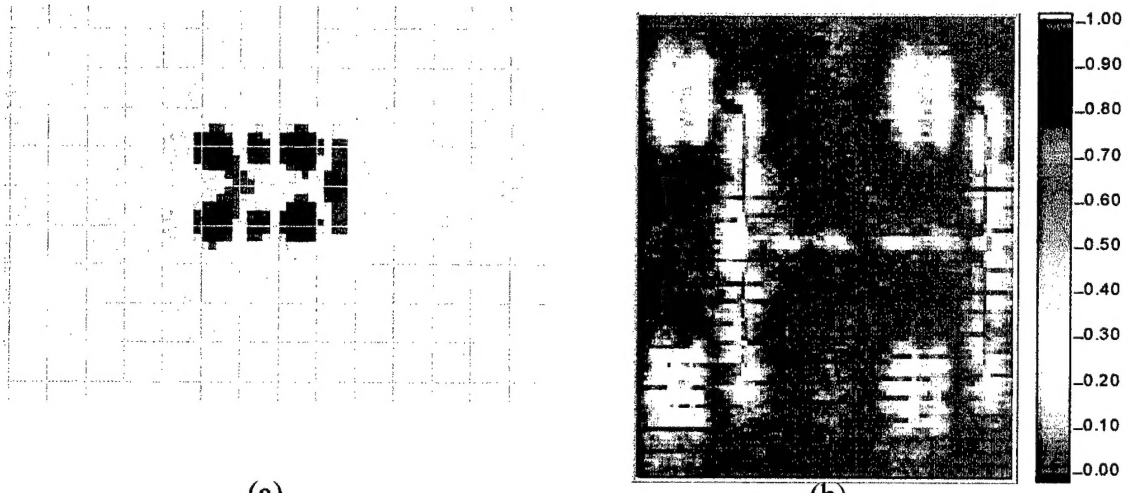

(a) (b)

Fig. 4. Comparison between image formed from near-field data and electro-optic image of a four-element array of microstrip patches.

References

1. P. L. Ransom and R. Mittra, "A method of locating defective elements in large phased arrays," in *Phased Array Antennas*, 351, *Proc. 1970 Phased Array Antenna Symp.* Dedham, MA: Artech House, 1972, p.351.

2. J. J. Lee, E. M. Ferren, D. P. Woollen, and K. M. Lee, "Near-Field Probe Used as a Diagnostic Tool to Locate Defective Elements in an Array Antenna," *IEEE Trans. Microwave Theory Tech*, vol. 36, No. 6, pp. 884-889, June, 1988.

3. G. David, K. Yang, W. Wang, L.W. Pearson, J.F. Whitaker, and L.P.B. Katehi, "3-D near-field analysis of a 4 x 4 grid oscillator using an electro-optic field imaging system," 1998 European Microwave Conference, Amsterdam, Netherlands.

4. K. Yang, S. V. Robertson, L.P.B. Katehi, and J.F. Whitaker, "Electrooptic field mapping of near-field distributions in integrated microwave circuits," *IEEE Trans. Microwave Theory Tech*, vol. 46, No. 12, p.2338-43, Dec. 1998.

5. Arthur D. Yaghjian, "Approximate Formulas for the Far Field and Gain of Open-Ended Rectangular Waveguide," *IEEE Trans. Antennas Propagat.*, vol. AP-32, p.378-384, April 1985.

Etched-Silicon Micromachined W-Band waveguides and Horn Antennas

Bassem A. Shenouda, L.Wilson Pearson, and James H. Harriss

Holcombe Department of Electrical and Computer Engineering
Clemson University
Clemson, SC 29634-0915
(864)656-3946 (voice & fax)
E-mail: bshenou@ces.clemson.edu, pearson@ces.clemson.edu, james.harriss@ces.clemson.edu

ABSTRACT

Micromachining of silicon is broadly proposed for the fabrication of substrates and waveguides at millimeter wavelengths. This paper presents the results of the fabrication of finned diamond-shaped waveguides and horn antennas by way of EDP anisotropic etching of silicon. The structure is fabricated in two halves by etching V-grooves in (100) silicon wafers. The etched faces of the wafers were metalized with gold. Metallic fins evaporated on a thin layer of mylar and sandwiched between the two halves of the structure were used to improve the bandwidth of the waveguide. Measurements were taken of the dispersion curve of the waveguide with fins with different gap separations, and of the radiation patterns of the fabricated horns with different flare angles at different frequencies. Measurements showed a very good agreement with numerical calculations using FEM technique. Computed attenuation curves for the structure are provided, as well.

I. INTRODUCTION

The realization of a diamond horn antenna in etched silicon has been suggested by Guo [1] and by Johansson and Whyborn [2]. A diamond-shaped structure arises naturally through wet-etch micromachining of (100) silicon wafer. The waveguide walls are aligned with (111) crystal planes, and the flare of the horns is a fine-scale corrugation of triangular cross-sections all characterized by the 70.52° angle between the (111) planes. However, since the etch rates in directions other than the <100> direction are not zero, the final shape of the horns does not exactly follow the mask used in the fabrication. Optical measurements are used to determine the actual flare angle of the fabricated structure and the dimensions of the horn opening. The measured dimensions are used in the numerical calculations.

II. FABRICATION

The antenna/waveguide assemblies depicted in Figure 1 were formed by etching 3 mm-thick (100) silicon wafers using EDP etchant properties indicated in [3]: namely, 150 cm^3 ethylene-diamine, 48 g pyrocatechol, 48 cm^3 water, 0.9 g pyrazine. The wafer was masked as indicated in Figure 2 to fabricate 3 waveguide/horn assemblies with different horn flare angles. The masked wafer was etched under agitation in the EDP solution at a temperature of 110° C for a time period that produces the desired etching depth at the deepest point inside the horn (2.5 mm) divided by the etch rate in the <100> direction (100 μm/hr). The width of the channels in the mask in Figure 2 is slightly less than the desired width of the final fabricated structure to compensate the effect of the etch in the <111> direction (2 μm/hr). Two clamshells are formed by sawing the etched wafer at the

opening of the horn. The different horns were sawed to have the same length so the horns with big flare angles would have bigger aperture areas. That was done after sawing the wafer in the longitudinal direction to separate between the different pairs of channels. For W-band operation, the lengths of the diagonals of the fabricated waveguides were 1.92 and 2.72 mm with the shorter length along the interface between the two halves. The structure was coated in thermal evaporator with gold to give a thin conducting layer, then it was electroplated with a layer of gold of approximately 6 times the skin depth at the operating frequency (6×0.25 μm). Aluminum fins were formed through on a thin mylar membrane which was sandwiched between the two halves of the structure. The wafer thickness limits the size of the aperture realized. The work reported here was done to investigate the concept of etching flare angles that do not align with crystal planes. Thicker wafers obviously can be used to achieve larger horn apertures.

III. MEASUREMENT JIG

Brass waveguides were machined to provide a smooth transition from the micromachined diamond-shaped waveguide to the standard rectangular waveguide used in the measurements. Figure 3 shows two pairs of jigs with the metalized micromachined waveguide in place. The metallic fins were tapered inside the brass waveguide to minimize reflection. This setting was used for the dispersion curve measurements of the waveguide. For the radiation pattern measurements, only one pair of jigs was used and the micromachined waveguide was replaced by the waveguide/horn assembly. The metallic fins were tapered inside the horn.

IV. MODELING AND RESULTS

We performed numerical calculations using the FEM technique with edge-based vector basis functions to determine the cutoff frequencies of the waveguide and the field distribution for each propagating mode. In the traditional fashion, the cutoff wavenumbers are the eigenvalues of the FEM system and the modal field distribution results form the associated eigenvectors. Figure 4 shows the field distribution of the first two propagating modes in diamond-shaped waveguide, and the first mode in a finned waveguide. The first two modes for the diamond-shaped waveguide counterparts to the TE_{10} and the TE_{01} modes in a rectangular waveguide. It is noted that the field lines of the second mode are perpendicular to the horizontal plane—the plane in which fins are to be placed. Consequently, the conducting fins will have no effect on this mode. On the other hand, the first propagating mode, with strong field component parallel to the plane of fins, will be strongly influenced by the presence of fins. The cutoff frequencies of the finned diamond-shaped waveguide are given in Table 1 for the first five modes and for different fin separations (g).

Table 1

N	No fins	g=1.22 mm	g=0.82 mm	g=0.64 mm
1	80.28 GHz TE	77.69 GHz TE	70.14 GHz TE	64.52 GHz TE
2	106.4 GHz TE	106.4 GHz TE	106.4 GHz TE	106.4 GHz TE
3	123.5 GHz TE	123.5 GHz TE	123.5 GHz TE	119.3GHz TE
4	133.5 GHz TM	137.8 GHz TM	129.4 GHz TE	123.5 GHz TE
5	183 GHz TE	162.5 GHz TE	141 GHz TE	134.3 GHz TE

The first cut-off frequency for the first mode decreases as the gap between the fins decreases, while the cut-off frequency for the second mode is unaffected by the fins. (The reason for this is clear from Figure 4b, where one observes that the field lines are transversely oriented at the fin sites.) Thus, the single-mode bandwidth of the guide can be adjusted by means of the fin separation.

Figure 5 displays the attenuation of several w-band waveguides as a function of frequency. The solid curve shows the attenuation of a diamond cross-section waveguide of the dimensions given in Section II. The attenuation of a standard gold WR-10 waveguide is shown with a dashed line. The third curve in the figure is the attenuation of the diamond cross-section guide with fins added so that the cutoff frequency of the dominant mode is 59 GHz, the same cutoff as WR-10 waveguide. It is seen that the attenuation curves for the finned diamond guide and for WR-10 are virtually identical. We have made a number of additional attenuation calculations that reveal that any variant of the diamond waveguide exhibits attenuation comparable with that of WR-10 so long as the dominant-mode cutoff frequencies of the two guides agree. Variations in the conductivity of the fins and in the cutoff frequency for the second propagating mode affect the attenuation only weakly.

V. MEASUREMENTS

Finned waveguides have been fabricated for a number of fin separations. Dispersion curves have been measured for these waveguides and compared with the calculated dispersion curves. These results are shown in Figure 6. One can infer from these curves, errors in cutoff frequency ranging from 1-3%. The radiation patterns were taken of the horns with different flare angles at 94 GHz. The angles of the fabricated horns were measured and found to be equal to 8.5°, 17°, and 22.5°. Tapered fins, with a gap separation of 0.6 mm in the waveguide, were used to take radiation pattern measurements at 75 GHz. E- and H-plane radiation patterns of these measurements with the calculated patterns are shown in Figures 7-10. We conclude from these figures that the radiation patterns get narrower for the horn with the big flare angle, which corresponds to a big aperture area. We can also see that the patterns measured at 94 GHz are narrower than the ones measured at 75 GHz which is expected since the electrical dimensions of the aperture become relatively large compared to the wavelength at higher frequencies. From our measurements of the radiation patterns of the finned structure at 94 GHz, we concluded that using the fins lowered the cutoff frequency of the waveguide

without any significant effect on the radiation patterns. The comparison between the measured and the calculated patterns in general shows a good agreement.

VI. CONCLUSIONS

W-band micromachined waveguides and horn antennas were fabricated using EDP anisotropic etching of silicon. Measurements of the dispersion curves were taken for finned waveguides with different fin separations. These measurements were compared to those calculated using FEM technique, and the comparison showed a good agreement with an error in cutoff frequency of less than 3 %. Radiation pattern measurements of horns were taken at 94 GHz before using the fins, then at 75, and 94 GHz after using fins in the structure to lower the cutoff frequency of the waveguide. Comparison between the measured and the calculated patterns showed a good agreement. The fin structure can be transitioned into coplanar waveguide for integration with monolithic system components.

ACKNOWLEDGMENTS

The authors wish to express gratitude to Dr. Yong Guo for his collaboration in the formative stages of this work. This work was sponsored by the U.S. Federal Aviation Administration under Grant Number 93-G-047.

REFERENCES

[1] Y. Guo, *Millimeter-Wave Integrated-Circuit Horn-Antenna Imaging Arrays,* Ph.D. Thesis, California Institute of Technology, August 1991.

[2] J. K. Johansson and N. D. Whyborn, "The Diagonal Horn as a Sub-Millimeter Wave Antenna," *IEEE Trans. MTT,* vol. 40, no. 5, pp. 795-800, May, 1992.

[3] X. Wu, Q. Wu and W. H. Ko, "A study on deep etching of silicon using Ethylene-Diamine-Pyrocatechol-water," *Sensors and Actuators,* 9, pp. 333-343, 1986.

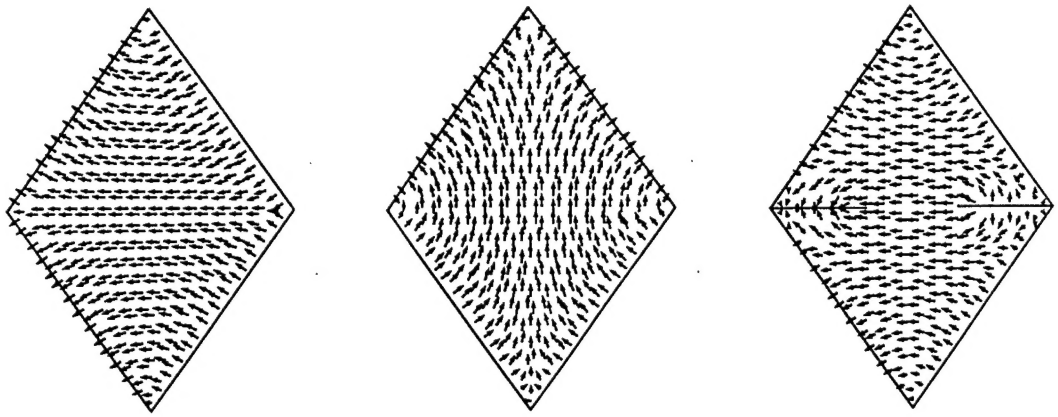

(a) (b) (c)

Figure 4. Field intensity representation for (a) first and (b) second propagating modes in diamond-shaped waveguide. Modification of the field pattern for the first mode in the presence of fins is shown in (c). Because the field lines of the second mode are normal to the fins, this mode is unaffected by the presence of the fin.

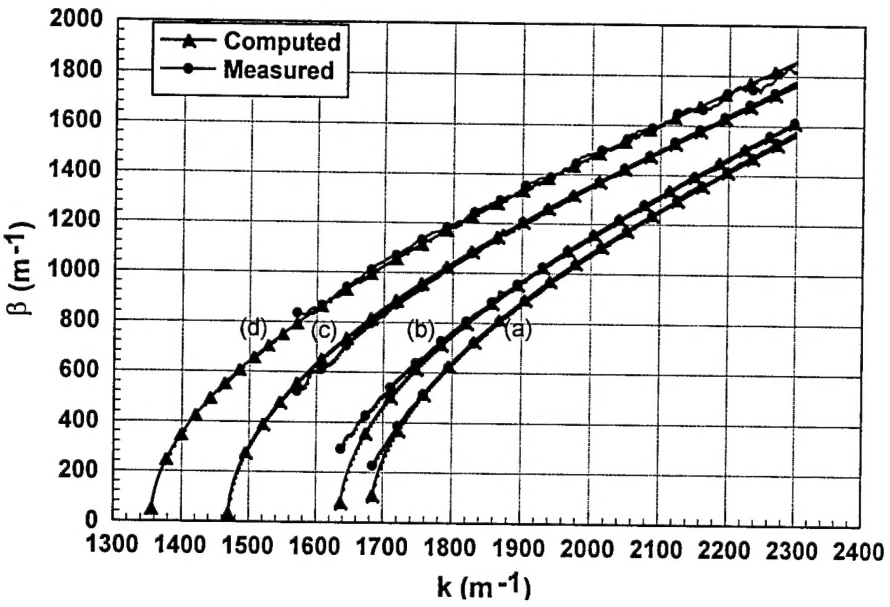

Figure 5. Measured and computed dispersion curves for the dominant mode in the finned diamond guide for four fin separations: (a) no fins, (b) g=1.22 mm, (c) g=0.82 mm, and (d) g=0.64 mm.

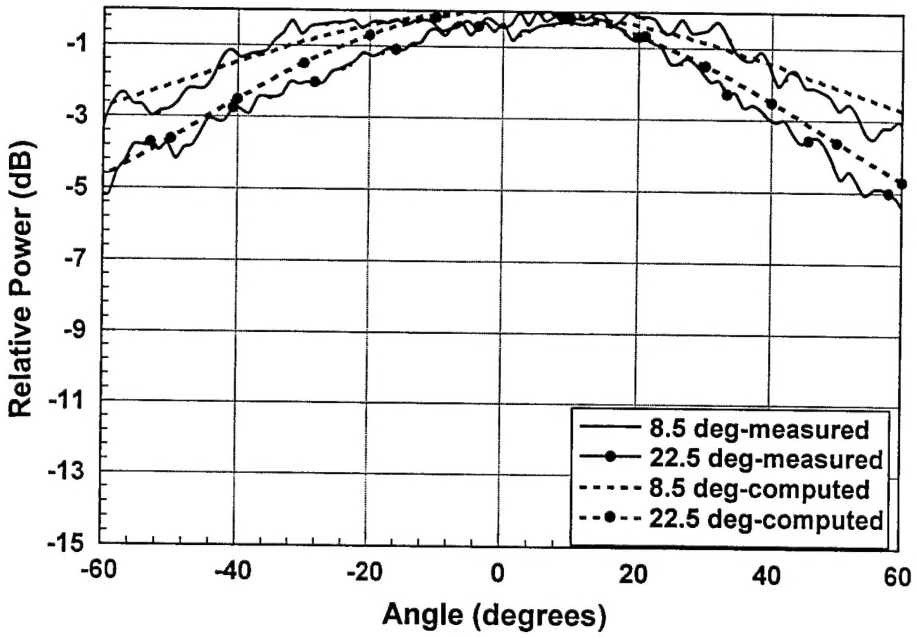

Figure 7. Measured and computed E-plane radiation patterns at 94 GHz of two different horns with flare angles of 8.5°, and 22.5°.